Chemiluminescence of Hydrogen Enriched Biogas Blends

Nuno Miguel Pina Bastos Rocha
nuno.bastos.rocha@tecnico.ulisboa.pt

Instituto Superior Técnico, Universidade de Lisboa, Portugal
November 2018

Abstract

Biogas utilization as a replacement of fossil fuels has been increasing. Hydrogen enrichment of biogas flames has been studied in recent years, as it has been found to improve combustion properties. Since biogas blends present variable compositions, a careful control of the H_2 amount added to the blend is required. Hence, chemiluminescence is presented as a possible method for flame monitoring.

An experimental and numerical study was conducted, to determine whether the hydrogen concentration (χ_{H_2}) and equivalence ratio (ϕ) of a hydrogen enriched biogas flame can be measured through chemiluminescence. Blends of CH_4/CO_2/air with $0 \leq \chi_{CO_2} \leq 30\%$ were studied in stoichiometric and lean conditions ($0.82 \leq \phi \leq 1$).

Analysis of flame morphology and area were also conducted. The spectra of flames were studied and methods for measuring radicals' intensities were proposed. The chemiluminescence of OH^*, CH^*, C_2^* and CO_2^* is thoroughly analysed with emphasis on chemiluminescent ratios.

It was shown that the OH^*/CH^* and CO_2^*/CH^* ratios may be options for χ_{H_2} measurement. The ratios OH^*/CH^*, OH^*/C_2^* and CH^*/C_2^* were shown to be good indicator of ϕ.

Keywords: Hydrogen, Biogas, Chemiluminescence, Premixed Flames

1 Introduction

Hydrogen is a fuel widely used in combustion applications, from cars, to domestic appliances, to spacecraft engines. Besides being a renewable energy resource, the main advantages of hydrogen over traditional fuels are its burning properties: high heat release rate, high laminar flame speed and wide flammability limits. One of the recent uses of hydrogen has been the enrichment of biogas to increase the quality of the fuel. Biogas, also a renewable resource obtained through anaerobic digestion (AD) has been used as an alternative to fossil fuels for some time. Substrates used for AD can come from a variety of sources such as agricultural waste, manure, sewage, landfill waste, algae or even plankton [1]. Although the main components of biogas are CH_4 and CO_2, appearing in the ranges $40-95\%$ and $5-55\%$, respectively, blends from different sources can present different compositions, containing a collection of other species in noteworthy amounts: hydrogen (H_2), nitrogen (N_2), oxigen (O_2), carbon monoxide (CO), hydrogen sulfide (H_2S) and ammonia (NH_3).

Biogas has been shown to display poorer flame properties than traditional fuels such as methane and natural gas. Pizzuti *et al.* [2] compiled results from a large number of works with a wide variety of biogas compositions and techniques. Biogas blends featured CO_2 content ranging from 0% to 60% and N_2 content between and 0% to 12.9% along with other minor species. In general, laminar flame speed, S_L, tends to decrease and flammability limits tend to narrow when the dilution with CO_2 and N_2 increases. Mixtures of hydrogen and biogas have been studied extensively [3, 4]. Zhen *et al.* [4] studied a variety of biogas blends with hydrogen enrichment ranging from 10% to 50% and concluded that not only the flammability limit increased, but that there was also an increase in laminar flame speed, flame tip temperature and more efficient oxidation of CO into CO_2. Biogas composition, as stated before, is highly variable and can change with the season, the substrate as well as with the anaerobic bacteria and method of production. For this reason, careful control of both air and fuel feed are necessary to hold a stable flame in lean conditions, as well as prevent acoustic instabilities, soot formation and emission of pollutants [5].

Chemiluminescence, the spontaneous light emission from excited species, has been used to determine important properties such as the equivalence ratio. In hydrocarbon flames, the main narrow-band emitters are OH^*, CH^* and C_2^* [6], while it has been suggested that the CO_2^* radical is responsible for a continuum across the UV-visible region of the spectrum (* denotes excited species) [7]. Radicals emitting in narrow bands display intensity peaks in the following wavelengths: OH^* centered at 309 nm, CH^* at 430 nm and C_2^* at 515 nm. The broadband continuum, despite featuring emission from various radicals, is generally attributed to CO_2^*. It extends from near-UV to the visible region [8].

Although modelling of combustion kinetics has been used extensively as of late, the chemiluminescent species and underlying mechanisms are seldom considered because of their high computational cost. For this reason a chemiluminescent mechanism was compiled by Kojima *et al.* [9] based on works on

formation and consumption of OH^*, CH^*, C_2^* and CO_2^*. Quintino *et al.* [5] have used this mechanism for biogas flames and found good agreement with experiments while Guiberti *et al.* [10] have used a similar set of equations, with some alternations in the kinetics parameters for OH^* and CH^* chemistry. The C_2^* kinetics were not included in their mechanism as the radical was also excluded from the experimental analysis. García-Armingol and Ballester, in their investigation, [11–13] have studied the chemiluminescence of major species in an array of fuel compositions containing CH_4, CO_2, CO and H_2. The OH^*/ CH^* ratio has been found to be a good tracker of ϕ in CH_4/CO_2 flames, as well as in methane flames [12]. In hydrogen-enriched methane flames, the measuring of ϕ was found to be highly dependent on the enrichment amount.
Ballester *et al.* [13] used a neural network to predict the composition of NG/H_2 flames based on flame spectra. Recently, Quintino *et al.* [5] have shown that various ratios can be used to infer the amount of CO_2 in a biogas flame (CH_4/CO_2) with the OH^*/CO_2^* and C_2^*/CO_2^* ratios displaying both the best agreement with simulations as well as good sensitivity and monotonicity. OH^*/CO_2^* has also been presented as a tracer of carbon dioxide in biogas flames [10].
The preset study has two main objectives: i) determine whether the amount of H_2 in a CH_4/CO_2 flame can be determined using chemiluminescence alone; ii) verifying whether chemiluminescent ratios previously used to measure the equivalence ratio of biogas flames, are still viable when the flames are enriched with small amounts of hydrogen. In Section 2 the experimental setup, procedure and data processing are described. Modeling and simulations are addressed in Section 3 while results are presented and discussed in Section 4. A summary and some conclusions are presented in Section 5.

2 Experiment

2.1 Setup

The experimental setup, displayed in Figure 1, is composed of two main systems: a burning flame system and a data acquisition system. The burning flame system is composed of the gas bottles, air line and burner, along with all components to connect and control the system, such as flow meters, mixing chambers, etc. The data aquisition system is composed of the camera and lens, the spectrometer and optical fiber, the computer and all the connecting cables.
The gases CH_4, CO_2 and H_2 were stored in three research grade bottles (with a purity of at least 99.95%). The air was extracted from the atmosphere and underwent filtering and desiccating before being fed to the burner. Each gas/air line was connected to a flow controller (Alicat Scientific, 16 Series) with maximum capacities of 20, 5, 1 and 0.5 SLPM for *air*, CH_4, CO_2 and H_2, respectively. The flame was stabilized on a Bunsen burner designed to hold a stationary, laminar, top hat flow. The mixture enters at the bottom section through four tangential inlets and is homogenized. It then proceeds through the middle section, where successive structures of small spheres and sintered glass improve the mixing of the reactants. The homogenized flow enters the top section and passes through a set of honeycombs, which act as a quenching net. A contraption, responsible for reducing the boundary layer effect to a to a point where it is negligible, follows. The profile of the contraption is given the equation: $y = (-10\zeta^2 + 15\zeta^4 - 6\zeta^5)(y_i - y_0) + y_i$, where $\zeta = \frac{z}{L}$ is the axial coordinate and L the length of the nozzle. The nozzle at the outlet is 20 mm wide and 0.2 mm thick.

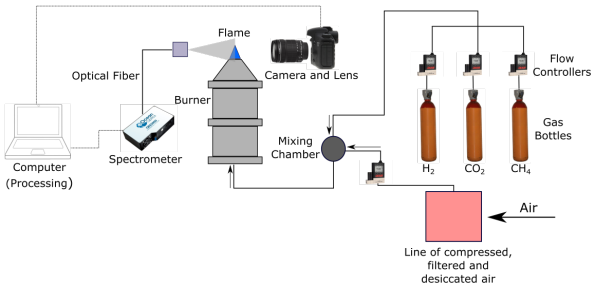

Figure 1: Experimental Setup.

The data acquisition system is divided in two branches: spectroscopy and photography. The spectrum was acquired by a 2 m long, 200 µm core diameter optical fiber (Ocean Optics, model QP400-2-SR-BX) with an average acceptance angle of 25.4°, connected to a spectrometer (Ocean Optics, model QE65000) through a 100 µm wide slit. The high sensitivity spectrometer collects light in wavelengths in the range [200, 1100]nm with an optical resolution of 3 nm. It was then connected to a computer and was operated using the Spectra Suite software. The optical fiber tip was placed perpendicularly to the flow direction, in a position as to capture the whole flame volume for all flame conditions studied (∼150 mm away from the flame). The camera (Canon EOS 7D) and respective lens (Canon EF-S $18-135$ mm) were positioned similarly to the optical fiber (perpendicularly to the flow and capturing the whole flame volume). It was also connected to the computer and was operated using digiCamControl software.

2.2 Procedure

The compositions were calculated maintaining the flame power constant at 750 W. In all experiments the biogas composition was fixed while the equivalence ratio and hydrogen enrichment percentage were varied. Each biogas blend was simulated

using a mixture of methane and carbon dioxide and is identified throughout this work by the letters 'BG' followed by its percentage of methane (ex: BG90 is 90% methane and BG100 is pure methane). The percentage of carbon dioxide in the biogas is defined by the following equation:

$$\chi_{CO_2} = \frac{Q_{CO_2}}{Q_{CH_4} + Q_{CO_2}} \quad (1)$$

This definition of χ_{CO_2} was chosen because it is considered that in an application where real biogas is used, its composition is defined before any hydrogen enrichment. The percentage of hydrogen is defined as the percentage in volume in the whole fuel mix, or in equation form:

$$\chi_{H_2} = \frac{Q_{H_2}}{Q_{biogas} + Q_{H_2}} = \frac{Q_{H_2}}{Q_{CH_4} + Q_{CO_2} + Q_{H_2}} \quad (2)$$

Biogas blends (including pure methane) were first burned in stoichiometric conditions ($\phi = 1$) and the $\chi_{H_2(\%)}$ was incremented in steps of 1% from 0% to 10%. The flame was submitted to the same procedure at a new ϕ of 0.9. At predefined $\chi_{H_2(\%)}$ set points of 0, 5 and 10 the equivalence ratio was decremented in steps of 0.02 until the lower flammability limit was found. Figure 2 summarizes the flammability limits of all biogas blends enriched to 0, 5 and 10 hydrogen percentage.

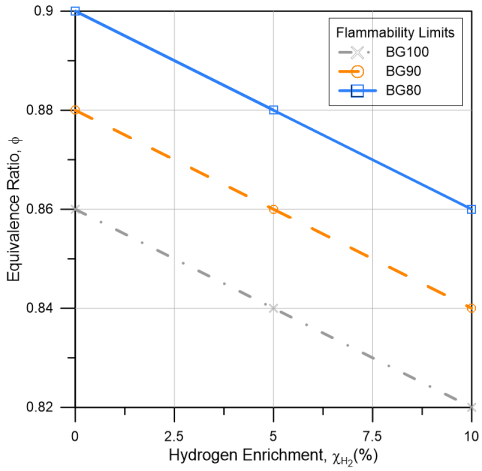

Figure 2: Stability analysis for each $CH_4/CO_2/H_2$ mixture.

The lean stability limit decreases with increasing hydrogen amount while it increases for increasing carbon dioxide dilution. BG80 displays the highest limit at $\phi = 0.9$ with no added H_2 and BG100 displays the lowest limit at $\phi = 0.82$ for maximum enrichment. Since $\chi_{H_2(\%)} = 10$ was the maximum considered under this study, no stable flame was obtained at $\phi = 0.8$.

Flame spectra were obtained by averaging at least 100 consecutive spectra with an integration time of 100 ms. The maximum uncertainty was calculated for the wavelengths corresponding to the peaks of each radical and never exceeded $\sim 8\%$. Furthermore, for each flame, 5 consecutive pictures were taken with the following camera set points: ISO 3200, shutter speed 1/320 and aperture 6.3. Each colored picture was then processed in a homemade MATLAB© routine to detect and calculate the area of the flame front. The uncertainty of the flame area calculation was studied for the tallest (BG80, $\phi = 0.9$, $\chi_{H_2} = 0\%$) and shortest (BG100, $\phi = 1$, $\chi_{H_2} = 0\% = 0\%$) flames, using a set of 25 images for each. Area uncertainty never surpassed $\sim 3\%$. Chemiluminescent ratio uncertainty never surpassed $\sim 7\%$

2.3 Data Processing

Spectra Processing

Spectra collected as described in Section 2.2 were further processed to extract the intensities of each radical. A scheme of the method can be found in Figure 3.

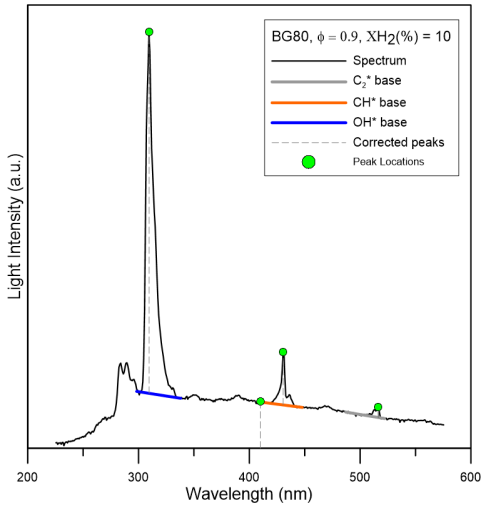

Figure 3: Corrected Peaks method for calculation of radicals intensities.

For OH^*, OH^* and C_2^* the intensity of the radical was defined as the difference between the local maxima and a band base. The base was calculated by fitting the intensities within each radical's border region to a linear function. The regions for local maxima and base bands can be found on Table 1.

Table 1: Band and base regions for calculating the maxima and base lines for OH^*, OH^* and C_2^*

Species	Band (nm)	Base Band (nm)
OH^*	[298, 338]	[298,301.4], [335, 338]
CH^*	[407.6, 448]	[407.6,411], [445, 448]
C_2^*	[486.6, 522]	[486.6,490], [519, 522]

The CO_2^* intensity was measured at a wavelength where no other radicals emit [410 nm]. This method was previously used before [5], and

displayed the best agreement with numerical data. García-Armingol *et al.* [12] compared an array of chemiluminescence measuring methods and found background corrected data to show more consistent results than absolute peaks or areas.

Image Processing

The image processing routine performs a number of image cleaning and enhancing subroutines before applying the main algorithm for detecting the flame front. An illustration of the major steps is shown in Figure 4.

The routine starts by obtaining a gray scale image (Figure 4b) from the blue color channel of the colored flame image (Figure 4a). The gray scale image is then cleaned of isolated groups of pixels, as is standard procedure in image processing routines. The gray image containing the whole flame region is then split vertically into two by the centroid. The flame front identification subroutine is then applied to each flame front half.

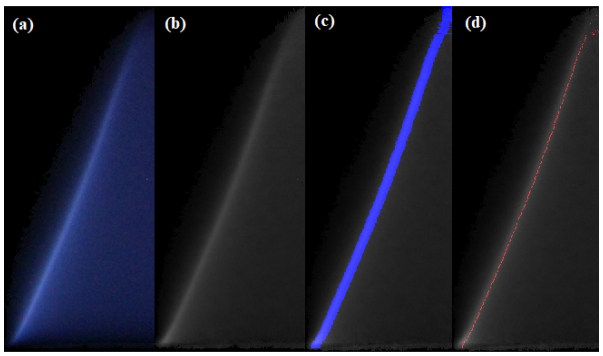

Figure 4: Image processing illustration. Pictures display only half of the flame cone. Left to right: true color, gray scale, detected flame front region (thick blue region) and flame front (red dots).

The flame region routine finds, in each row, the group of adjacent pixels with the highest total intensity. The collection of the groups will form the flame front region, displayed in 4c. The 'width' of this group, or number of pixels to form the group, can be changed to better fit the image resolution. The determination of the group width lies in the balance between sensitivity and continuity (e.g. if the group width is decreased, sensitivity should increase, however, if it's too thin it will do little to minimize the variation of a cheaper maximum intensity pixel routine). The center of the flame front region (middle pixel of each group) is the flame front. A typical flame front is displayed in Figure 4d.

Each flame front profile is then revolved around the vertical axis resulting in a approximately conical-shaped flame front surface. The resulting area is given by applying the trapezoidal rule to the flame front:

$$A_{Total} = L_{pixel} * \Sigma(d_{center}) * 2\pi \qquad (3)$$

where L_{pixel} is the length of the side of a pixel and d_{center} is the horizontal distance between each flame front pixel and the axis of the flame picture.

3 Modeling

Simulations were conducted using Cantera [14] (an open-source suite of tools for chemical kinetics, thermodynamics and transport processes) on the programming language PYTHON. The combustion mechanism used was a version of GRI 3.0 excluding the nitrogen kinetics, to reduce processing time. A chemiluminescent mechanism comprising the kinetics of CH^*, OH^*, C_2^* and CO_2^* based on a number of works compiled by Kojima *et al.* [9] was appended to the combustion one. A thorough explanation of the mechanism can be found elsewhere [5]. The Cantera routine calculates a one-dimensional free flame set within a predefined grid. Initial conditions were set at 1atm and 298K. The grid, aligned with the flame propagation direction, z, is continuously refined until a solution is found within the tolerance parameters. The result is the temperature, pressure and concentration of all species, at every node along the z direction. The solution is then processed in a homemade MATLAB© routine. Concentrations are calculated node-wise for each chemiluminescent species. The light intensity is given by Equation 4:

$$I = \int_{z_0}^{z_f} k_i [X^*]_z dx \qquad (4)$$

where z_0 and z_f are the initial and final coordinates of the grid, k_i is the Einstein coefficient of light emission for the reaction i and $[X^*]$ is the chemiluminescent species', X, concentration at z coordinate. The reaction rate for the equation $X^* \rightarrow X$ is given uniquely by the pre-exponential factor, A, as the temperature dependent terms on the Arrhenius form[1], E and β, are null. The integration was performed numerically, using the trapezoidal rule, and yielded results in light intensity per unit area [photons s^{-1} m^{-2}]. The intensity value considered is the result of the integration of light emission across the whole domain for coherence with the experimental method.

4 Results and Discussion

4.1 Flame Morphology

Premixed, laminar hydrocarbon flames, obtained in a top-hat flow burners are generally cone shaped and present a blue color. Figure 5 contains pictures of pure methane flames enriched with hydrogen up to 10%, at various equivalence ratios. Pictures, which are in true color, were taken with the camera in a fixed position and no further processing was applied. Figure 5a contains a set of methane

[1] Arrhenius form: $k = AT^{\beta}e^{-\frac{E}{RT}}$

flames, enriched at fixed $\chi_{H_2}(\%) = 5$, with equivalence ratios increasing from 0.84 to 1.
Two changes in flame characteristics are immediately noticeable when decreasing equivalence ratio: the flame height increases and light density (light intensity per unit area) decreases. In this case, flame area can be defined as a balance between the reactants flow speed and flame burning velocity, as described in Equation 5.

$$\int_{A_{\text{section}}} V_{\text{reactants}} dA = \int_{A_{\text{flame}}} S_L dA \qquad (5)$$

where A_{section} is the area of the burner exit, $V_{\text{reactants}}$ is the velocity of the reactants flow, S_L is laminar flame speed and A_{flame} is the flame area. When a constant velocity across the the flow section and constant S_L are assumed, it takes the following form:

$$V_{\text{reactants}} * A_{\text{section}} = S_L * A_{\text{flame}} \qquad (6)$$

Selected flame area results are displayed in Figure 6 against flame conditions.

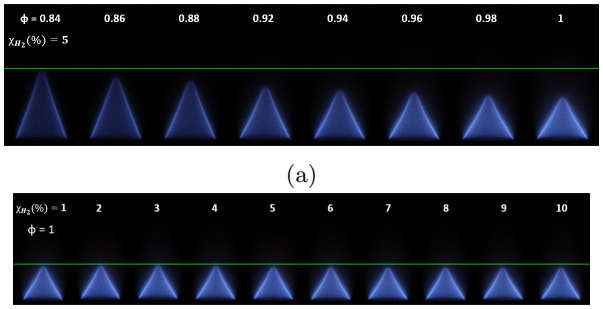

(a)

(b)

Figure 5: Pictures of pure methane flames burning in: $0.82 \leq \phi \leq 1$, with hydrogen content of: $0 \leq \chi_{H_2}(\%) \leq 10$. Green horizontal lines are positioned at the highest vertical flame coordinate of each set.

For biogas compositions up to 20% in CO_2 and H_2 enrichment setpoints of 0%, 5% and 10% (Figure 6a), flame area increases with decreasing equivalence ratio. An increase in flame area with decreasing ϕ has been reported for biogas flames within the operation conditions of this study [4]. The decrease in light density may be attributed to the increase in flame area and ensuing dispersion of light emission radicals across a larger region.

The bottom set (Figure 5b) contains pictures of methane flames burning in stoichiometric conditions enriched with $\chi_{H_2}(\%)$ in steps of 1% up to 10%. The figure shows a very small decrease in flame height. Flame area calculations for methane and biogas flames enriched with hydrogen up to 10%, burning at $\phi = 1$ are presented in Figure 6b. The measurements conclusively denote a small decrease in flame for all conditions when hydrogen in added to the base fuel.

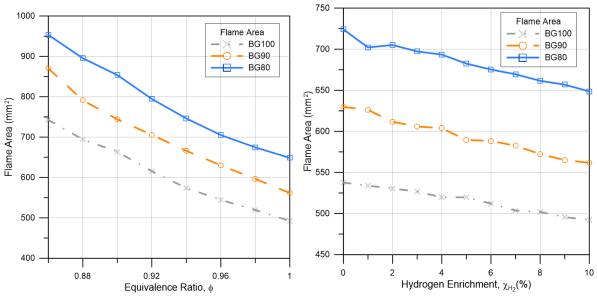

(a) Variable ϕ (b) Variable χ_{H_2}

Figure 6: Flame area for varying equivalence ratio and hydrogen enrichment. Crosses, squares and circles represent BG100, BG90 and BG80, respectively.

4.2 Global Spectral Analysis

Figure 7 displays the emission spectra from BG80 flames enriched with hydrogen up to 10%.

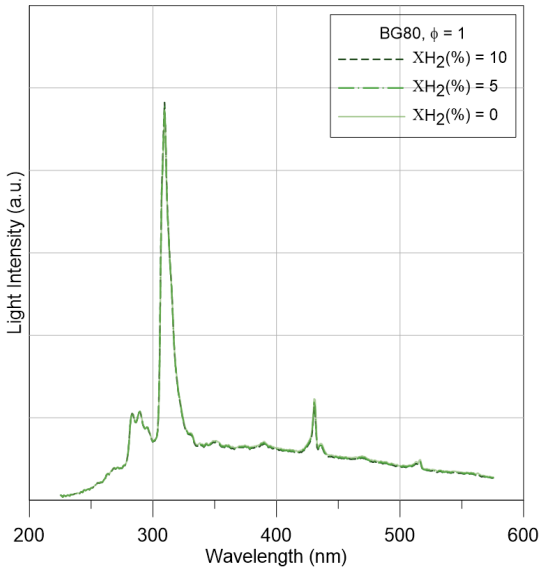

Figure 7: Superimposed CH_4/CO_2/air flame spectra for $\chi_{H_2}(\%) = 0, 5, 10$ at equivalence ratios of 1. Solid light lines represent biogas with no H_2, dot-dashed lines represent biogas with $\chi_{H_2}(\%) = 5$ and dashed dark lines represent biogas with $\chi_{H_2}(\%) = 10$.

The first noteworthy fact is that there is little visual variation with the addition of hydrogen in the BG80 flame. However, integrating the spectra over the [225nm - 575nm] domain shows that the total intensity does in fact decrease when hydrogen percentage is increased from 0 to 10% by about 4% and this value increases to 6% when the spectra are corrected for flame area.

Figure 8 displays superimposed spectra of biogas flames enriched with $\chi_{H_2}(\%) = 10$, for a range of equivalence ratios, ϕ. As expected, there is a decrease in global spectral light intensity with the decrease of equivalence ratio, in lean conditions. Par-

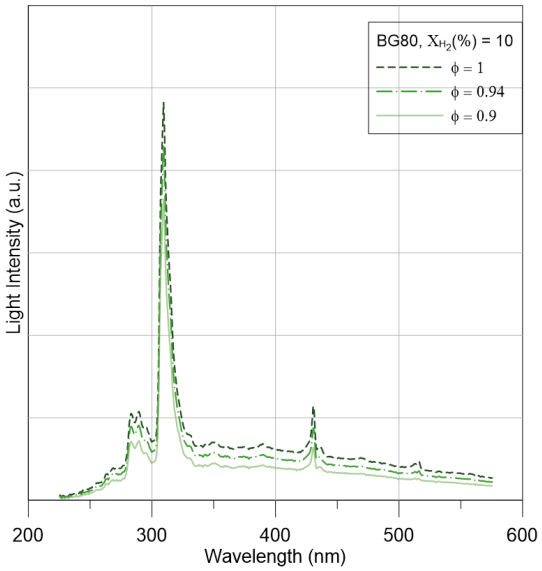

Figure 8: Superimposed$CH_4/CO_2/H_2$/air flame spectra at equivalence ratios ranging from 0.9 to 1 and $\chi_{H_2}(\%) = 10$. Solid light lines represent flame at minimum ϕ, dot-dashed lines represent at ($\phi = 0.94$) and dashed dark lines represent flames at $\phi = 1$.

ticularly for biogas flames, this has already been verified by Quintino *et al.* [5]. The decrease in total light intensity has been reported for methane flames [11] as well as natural gas flames [13], both enriched with hydrogen up to 50%.
The intensity appears to decrease proportionally throughout the spectrum. The shape of the spectra in the OH* and CH* regions remains approximately the same with the decrease of equivalence ratio, an effect which was also reported by García-Armingol and Ballester [11]. The decrease in the C_2^* region, however, is not proportional to the other species. Its intensity decreases much more than the surroundings, resulting in local maxima of very small magnitude. The decrease in C_2^* intensity has been reported to decrease faster than other radicals, even in lean conditions, as reported by Quintino *et al.* [5]. The decrease of CO_2^* background emission is in line with many authors [5, 10, 11, 13].

4.3 Effect of H_2 enrichment in OH* and CO_2^* chemiluminescence

Although single chemiluminescent radicals are generally not used in measuring flame properties, understanding how their intensities vary with the measured conditions can be relevant for the study of combustion kinetics. An example of this variation is displayed in Figure 9 for OH* and CO_2^*.

Figure 9a displays the variation of OH* with $\chi_{H_2}(\%)$. A visual analysis shows that there is a noticeable increase of OH* intensity with hydrogen content for all compositions. Despite a following a relatively steeper line, the experimental tendencies is closely followed by the numerical data for BG100. For increasing amounts of CO_2 in the biogas, the experimental curves become steeper. Although there is some under prediction in the simulations, the trend of steeper curves with increasing CO_2 is maintained.

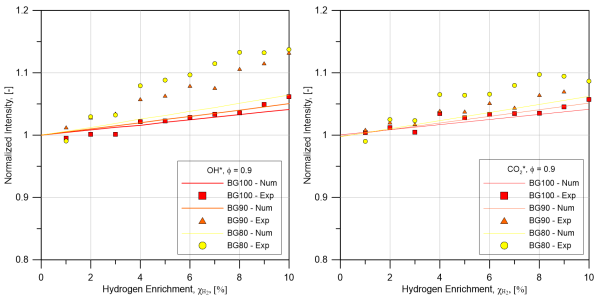

(a) (b)

Figure 9: Normalized Intensities of OH* and CO_2^* radicals vs $\chi_{H_2}(\%)$ for biogas with χ_{CO_2} ranging from 0% to 20%. All intensities were normalized by their respective values at $\chi_{H_2} = 0\%$. Fuel compositions present in these charts were burnt at $\phi = 0.9$. Lines represent numerical simulation and symbols experimental results.

The CO_2^* intensity shows a linear increase with $\chi_{H_2}(\%)$ for all biogas compositions. Relatively good agreement between numerical and simulated data was found as all curves show a small increase in intensity of $5\% \sim 10\%$ when χ_{H_2} is increased by 10%. Here, the tendency of increasing steepness with CO_2 content is also verified for both experimental results and simulations.

4.4 H_2 assessment using OH*, CH*, C_2^* and CO_2^* chemiluminescent intensity ratios

With proper calibration, under known flame conditions and for a single burner, the usage of a single radical could be used to track flame variables, such as ϕ or heat release rate [15]. However, if a single flame condition (such as the flame area, power, burner configuration, strain rate, etc.) were to change, it would be no longer possible to measure the chosen variable. With this in mind, the use of chemiluminescent ratios has been proposed, as they have been shown to be relatively independent of flame area [6, 16].
Figure 10 diplays the OH*/CH* ratio against $\chi_{H_2}(\%)$ at $\phi = 1$. Numerical simulation lines are also present for biogas compositions between BG100 and BG70. The pure CH_4, or BG100, curve displays a steady increase of $\sim 14\%$ when the flame is enriched with hydrogen from 0% to 10%. The ratio exhibits relatively good agreement between simulations and experimental data for all biogas compositions.
When pure methane is replaced with biogas, the

slope of the numerical line increases with increasing amounts of CO_2. This effect is verified experimentally, with values displaying a larger variation with larger CO_2 content. Although good agreement between numerical and experimental data and injective behavior were verified for the OH^*/CH^* ratio, the relatively low sensitivity to the variable ($\chi_{H_2}(\%)$) is a limiting factor in determining whether it could be used as a tracer. Further work is required to understand what level of certainty can be achieved in measuring $\chi_{H_2}(\%)$ in biogas flames withing the composition and equivalence ratio ranges of this research.

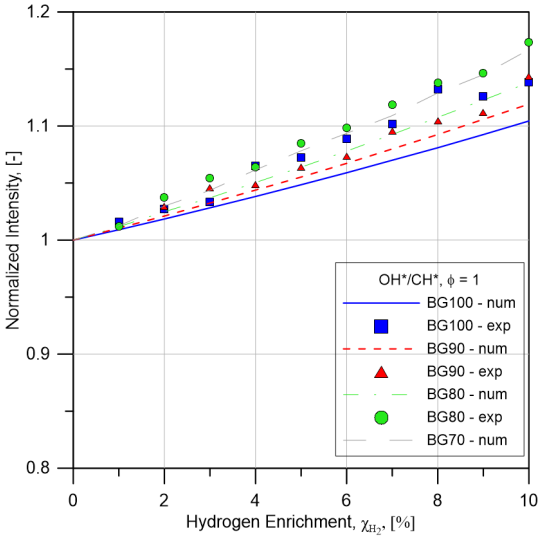

Figure 10: Normalized Intensity Ratio OH^*/CH^* vs $\chi_{H_2}(\%)$ for biogas with CO_2 content ranging from %0 to 30%. All intensity ratios are normalized by their respective values at $\chi_{H_2}(\%) = 0$. Fuel compositions present in these charts were burnt in stoichiometric conditions. Lines represent numerical simulation and symbols experimental results.

Figure 11 shows the CO_2^*/CH^* intensity ratio vs $\chi_{H_2}(\%)$ for various methane and biogas compositions. Experimental results are present for biogas diluted with CO_2 up to 20% in volume, and simulations go up to $\chi_{CO_2} = 30\%$. The methane numerical curve displays a linear increase in intensity of $\sim 11\%$ with the addition of H_2 up to 10%. Despite displaying a large dispersion, the experimental results follow a similar tendency but with a smaller slope. For biogas with CO_2 dilutions of 10%, 20% and 30%, the numerical curves maintain an approximately linear behavior, with progressively larger slopes. The experimental data displays similar behavior: approximately linear variation with H_2 content with larger slopes for increased carbon dioxide. BG100 and BG90 display a smaller slope than the respective simulations, while BG80 values are with good agreement.

The CO_2^*/CH^* ratio might be a viable option in monitoring of $\chi_{H_2}(\%)$ in biogas flames, especially

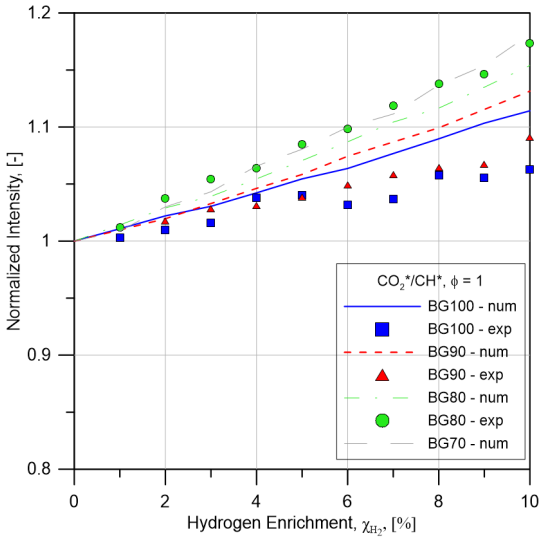

Figure 11: Normalized Intensity Ratio CO_2^*/CH^* vs $\chi_{H_2}(\%)$ for biogas with CO_2 content ranging from %0 to 30%. All intensity ratios are normalized by their respective values at $\chi_{H_2}(\%) = 4$. Fuel compositions present in these charts were burnt in stoichiometric conditions. Lines represent simulations and symbols experimental results.

for higher amounts of CO_2. It displays clear monotonicity for all compositions and increasing sensitivity with increased χ_{CO_2}.

4.5 Effect of ϕ on OH*, CH*, C_2^* and CO_2^* chemiluminescent intensity ratios

In this section, chemiluminescent ratios previously used to determine the equivalence ratio of biogas, are studied for mixtures enriched with χ_{H_2}.

Figure 12 displays both numerical and experimental values of OH^*/CH^* for equivalence ratios ranging from stoichiometric conditions downwards. The biogas CO_2 content was varied between 0% and 30% in simulations, and between 0% and 20% in experiments. All biogas presented were enriched to $\chi_{H_2} = 10\%$, with the exception of some simulated BG100 and BG90 compositions. Experimental values for these compositions are not presented as they have been extensively studied elsewhere and good agreement between numerical and experimental results was found [5]. These simulations were included in this work with the purpose of better comparing results with and without hydrogen enrichment.

In the studied range ($0.7 \leq \phi \leq 1$), the ratio intensity is known to decrease with increasing equivalence ratio [5, 6]. Curves displayed here all decrease at about the same rate and even overlap near stoichiometry. Not only no relevant difference is found for biogas blends with CO_2 contents varying from 0% to 30% and $\chi_{H_2} = 10\%$, as no significant change is noticed when the H_2 is set to 0, thus demonstrating that OH^*/CH^* is fairly independent of both

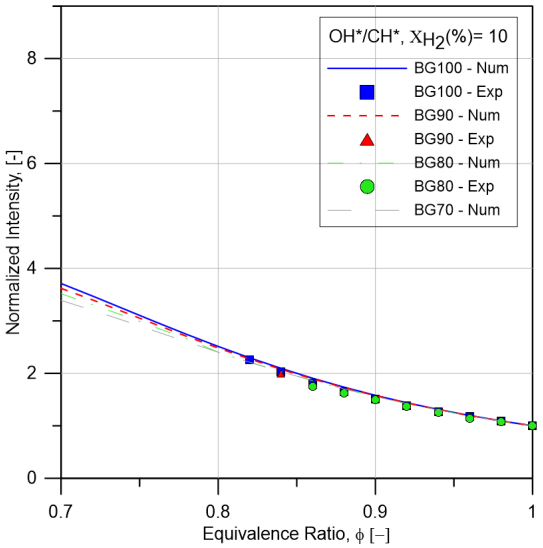

Figure 12: Normalized intensity ratio OH^*/CH^* vs ϕ for biogas with CO_2 content ranging from 0% to 30%. All intensity ratios are normalized by their respective values at $\phi = 1$. Fuel compositions present in these charts were burnt in at $\chi_{H_2} = 10\%$. Lines represent simulations and symbols experimental results. BG100 - blue solid line and squares; BG90 - red dashed line and triangles; BG80 - green dashed line and circles; BG70 - gray wide dashed line.

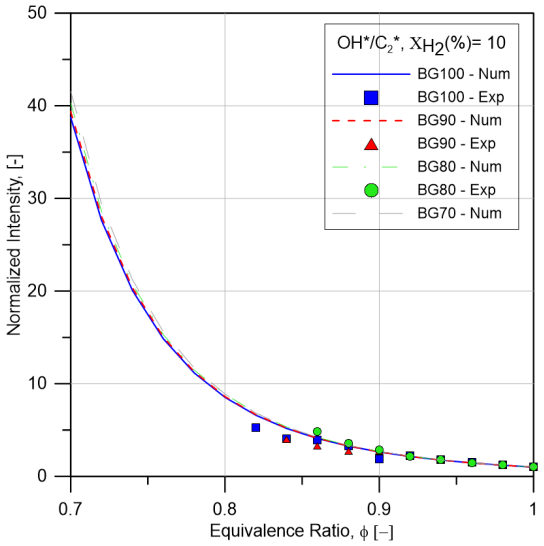

Figure 13: Normalized Intensity Ratio OH^*/C_2^* vs ϕ for biogas with CO_2 content ranging from 0% to 30%. All intensity ratios are normalized by their respective values at $\phi = 1$. Fuel compositions present in these charts were burnt in at $\chi_{H_2} = 10\%$. BG100 - blue solid line and squares; BG90 - red dashed line and triangles; BG80 - green dashed line and circles; BG70 - gray wide dashed line.

CO_2 and H_2 content in the base CH_4 fuel in the quantities previously mentioned. The plots display good agreement between simulations and experiments for compositions down to $\phi = 0.82$.

Figure 13 displays the results for the OH^*/C_2^* ratio. As shown previously [5], there is a steep increase in intensity from $\phi = 1$ downwards. This ratio displays the highest sensitivity of the three, with an expected intensity increase of 40 times from $\phi = 1$ to $\phi = 0.7$.

Figure 14 contains the CH^*/C_2^* variation with ϕ. The ratio's sensitivity is placed between the other two. As in OH^*/CH^*, variation in both OH^*/C_2^* and CH^*/C_2^* ratios with CO_2 content is negligible. The agreement with simulations for the latter two ratios is clearly worse than for the first one (OH^*/CH^*). The dispersion, however, is not constant across the whole equivalence ratio range, but increases for leaner conditions. It's especially interesting that the dispersion increases greatly beyond $\phi = 0.9$ (to the lower side). The main difference between Figure 12 and Figures 13 and 14 is the presence of the C_2^* radical. As mentioned previously in Section 4.4, this radical becomes significantly harder to measure when progressing to leaner flames, hence the increased dispersion of the data.
Given the relatively high sensibility and low dispersion, all three ratios should be able to predict the equivalence ratio of a fuel mixture. The monotonic behavior of all curves determines that, unlike other works where several ratios had to be measured [6], one ratio should suffice within the operational range studied. The precise measurement of ϕ would still depend on careful calibration.

5 Conclusions

The main goal of this work was verifying whether the H_2 amount can be measured using chemiluminescence alone. To this end, the OH^*, CH^*, C_2^* and CO_2^* radicals were studied in simulations and experimentally, and results from both sources were compared. Biogas compositions were considered in the range $\chi_{CO_2} \leq 30\%$ and burned in stoichiometric and lean conditions ($1 \leq \phi \leq 0.82$).
Parallel to the main goal, flame morphology and equivalence ratio tracking using chemiluminescence, studied in previous works, were verified under slightly different conditions. The main findings are:

1. The flammability limits of all biogas blends were extended when hydrogen was added to the mixture, and their extension increased with χ_{H_2}.
2. The height of biogas flames of all compositions decreased slightly with the addition of hydrogen, due to an increase in laminar flame speed, while the flame area increased for decreasing equivalence ratio. The Row Group Maxima detection mechanism presented in this study yielded better results than traditional Row Maxima methods.
3. Although spectra for hydrogen/biogas flames

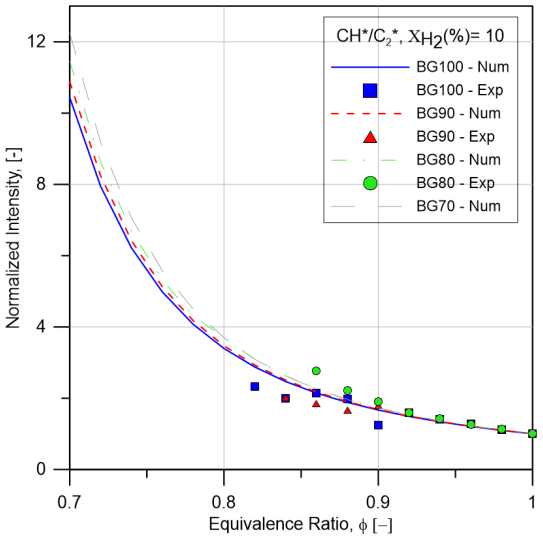

Figure 14: Normalized Intensity Ratio CH^*/C_2^* vs ϕ for biogas with CO_2 content ranging from 0% to 30%. All intensity ratios are normalized by their respective values at $\phi = 1$. Fuel compositions present in these charts were burnt at $\chi_{H_2} = 10\%$. BG100 - blue solid line and squares; BG90 - red dashed line and triangles; BG80 - green dashed line and circles; BG70 - gray wide dashed line.

display relevant variation with decreasing equivalence ratio, the effect of increasing the amount H_2 up to 10% is barely noticeable to the naked eye.

4. The OH^*, C_2^* and CO_2^* intensities decrease for increasing H_2 amount in the flame, while the CH^* decreases. Due to the small intensity of CH^* and C_2^* relative to their surrounding regions in the spectrum, their measurement displays a large dispersion.

5. The numerical predictions for OH^*, CH^*, C_2^* and CO_2^* using the extended mechanism were only fair, but the tendencies were correctly assessed.

6. The OH^*/CH^* and CO_2^*/CH^* ratios could be able to measure the hydrogen enrichment in a biogas flame as their tendencies were injective. However, the sensitivity of the curves was low and the dispersion high. Other radical combinations displayed less sensitivity and were, thus, discarded.

7. The OH^*/CH^*, OH^*/C_2^* and CH^*/C_2^*, previously shown to be able to measure ϕ in biogas, were verified to do so when hydrogen is added to the fuel up to 10%.

References

[1] D. Deublein and A. Steinhauser. *Biogas from waste and renewable resources: an introduction*. John Wiley & Sons, 2011.

[2] L. Pizzuti, C. Martins, and P. Lacava. Laminar burning velocity and flammability limits in biogas: A literature review. *Renewable and Sustainable Energy Reviews*, 62:856 – 865, 2016.

[3] T. Leung and I. Wierzba. The effect of hydrogen addition on biogas non-premixed jet flame stability in a co-flowing air stream. *International Journal of Hydrogen Energy*, 33(14):3856–3862, 2008.

[4] H. Zhen, C. Leung, C. Cheung, and Z. Huang. Characterization of biogas-hydrogen premixed flames using bunsen burner. *International Journal of Hydrogen Energy*, 39(25):13292 – 13299, 2014.

[5] F. Quintino, T. Trindade, and E. Fernandes. Biogas combustion: Chemiluminescence fingerprint. *Fuel*, 231:328 – 340, 2018.

[6] N. Docquier, F. Lacas, and S. Candel. Closed-loop equivalence ratio control of premixed combustors using spectrally resolved chemiluminescence measurements. *Proceedings of the Combustion Institute*, 29(1):139 – 145, 2002. Proceedings of the Combustion Institute.

[7] M. Kopp, M. Brower, O. Mathieu, E. Petersen, and F. Güthe. chemiluminescence study at low and elevated pressures. *Appl Phys B*, 107:529–538, 2012.

[8] T. Trindade. *Chemiluminescence spectral identity of premixed methane and propane flames*. PhD thesis, Lisbon University, 2015.

[9] J. Kojima, Y. Ikeda, and T. Nakajima. Basic aspects of oh (a), ch (a), and c2 (d) chemiluminescence in the reaction zone of laminar methane–air premixed flames. *Combustion and flame*, 140(1-2): 34–45, 2005.

[10] T. Guiberti, D. Durox, and T. Schuller. Flame chemiluminescence from co2- and n2-diluted laminar ch4/air premixed flames. *Combustion and Flame*, 181:110 – 122, 2017.

[11] T. García-Armingol and J. Ballester. Flame chemiluminescence in premixed combustion of hydrogen-enriched fuels. *International Journal of Hydrogen Energy*, 39(21):11299–11307, 2014.

[12] T. García-Armingol, J. Ballester, and A. Smolarz. Chemiluminescence-based sensing of flame stoichiometry: Influence of the measurement method. *Measurement*, 46(9):3084–3097, 2013.

[13] J. Ballester, R. Hernández, A. Sanz, A. Smolarz, J. Barroso, and A. Pina. Chemiluminescence monitoring in premixed flames of natural gas and its blends with hydrogen. *Proceedings of the Combustion Institute*, 32(2):2983 – 2991, 2009.

[14] D. G. Goodwin, H. K. Moffat, and R. L. Speth. Cantera: An object-oriented software toolkit for chemical kinetics, thermodynamics, and transport processes. `http://www.cantera.org`, 2017. Version 2.3.0.

[15] M. Orain and Y. Hardalupas. Effect of fuel type on equivalence ratio measurements using chemiluminescence in premixed flames. *Comptes Rendus Mecanique*, 338(5):241–254, 2010.

[16] J. Kojima, Y. Ikeda, and T. Nakajima. Spatially resolved measurement of oh*, ch*, and c2* chemiluminescence in the reaction zone of laminar methane/air premixed flames. *Proceedings of the Combustion institute*, 28(2):1757–1764, 2000.